Proceeding Paper

Examination of Two-Quadrant DC–DC Converter with Single-Ended LC Output Filter [†]

Vasil Mihov *[ID], Angel Lichev [ID], Yasen Madankov and Dimitar Spirov

Department of Electrical Engineering and Electronics, University of Food Technologies, 4002 Plovdiv, Bulgaria; a_lichev@uft-plovdiv.bg (A.L.); y_madankov@uft-plovdiv.bg (Y.M.); d_spirov@uft-plovdiv.bg (D.S.)
* Correspondence: v_mihov@uft-plovdiv.bg
[†] Presented at the International Conference on Electronics, Engineering Physics and Earth Science (EEPES'24), Kavala, Greece, 19–21 June 2024.

Abstract: This paper presents an examination regarding the DC–DC converter output behavior at variable loads. An example of a circuit with two-quadrant operation with different control methods is shown. The presented mathematical approach is used to determine the main output values and could have an enclosure as the calculation methodology. The examination data for the step-down circuit configuration with a single-ended output LC filter are provided. A modified excel model is used to extract the parameters for the circuit output gain at the rated frequency. The simulations of the load factor variation are shown in four different plots, where the area of the steady operation is presented. The results are derived to estimate the relationship between the circuit output and load characteristics' deviation. The converter dynamic range of the operation is determined by the presented graphics. A proper LC output filter design is essential for reducing the ripple currents and increasing the overall circuit effectivity.

Keywords: power converter; bidirectional energy transfer; DC chopper; LC filter

1. Introduction

In the present application, a two-quadrant DC–DC converter is also described as a DC chopper. It is a well-known fundamental switching circuit stage, and it is widely used in areas where bidirectional energy transfer is required—motor control with regenerative braking, battery charging in renewable energy systems, microgrid power distribution, and more [1,2]. With the application of various control methods, it is possible to obtain the energy transfer to the load and vice versa [3]. In practical implementations, there are two main circuit topologies: step-down and step-up DC–DC converters. The average quantities are adjusted when the switching state is controlled.

Different mathematical methods are used to calculate the main values of the ripple bias and voltage drop at the converter stage components [4,5]. A simple circuit topology with advanced control can obtain better results with a proper output filter setup. Nowadays, robust algorithms are used to increase the overall circuit efficiency [6,7]. Furthermore, in practice, there are some implementations where the control frequency is also variable [8]. This again requires an advanced approach in the circuit design in order to obtain proper electromagnetic field (EMF) and efficiency characteristics [9]. Adjustment of the output LC filter configuration and values could increase the overall circuit effectiveness [10].

Most of the above-quoted applications demand advanced circuit designs and complex control in order to obtain the required output parameters for each case. The presented study is focused on proper filter estimation. In many cases, the overall device characteristics are affected by the filter parameters. Considering this fact is crucial for applications with wide dynamic ranges and variable loads. More of these conditions are presented in practical implementations as battery charging, where the state of the charge and therefore its characteristics change in several instances. The authors examine the circuit output

behavior (the gain at the rated frequency) due to the load factor variation and extract the data for the converter steady state of the operation.

2. Circuit Topology and Calculation Methods

A DC–DC converter in which the power can flow from the source to the load and vice versa while the load voltage maintains the same polarity is referred to as a two-quadrant converter (Figure 1). In other words, the two-quadrant converter operates in the 1st and the 4th quadrants. Consider that the power can only flow from the load toward the source when the load has an active component such as a battery (battery charger system) or the back EMF of a DC electric drive.
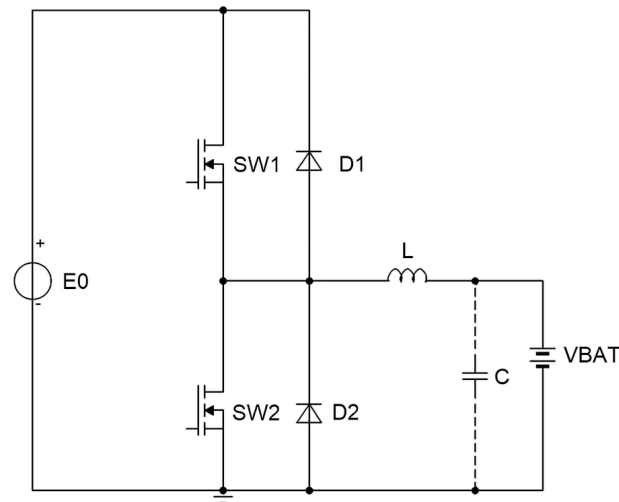

Figure 1. DC–DC converter (chopper) primary circuit.

Output voltage of the converter is normally regulated by two different methods, widespread in practice: pulse width modulation control (PWM) at constant frequency operation or variable frequency control (VF). For PWM control, t_{on} is changed while keeping operating frequency f and period T constant. Output voltage is varied by adjusting the ON time t_{on}. Pulse sequence for this method is shown in Figure 2a. For VF control, operating frequency f' is changed, keeping either t_{on} or t_{off} constant. To obtain full output voltage range, frequency has to be varied over a wide range. This method produces huge number of harmonics in the output, and for large t_{off} output current may become discontinuous. Pulse sequence for this method is shown in Figure 2b:
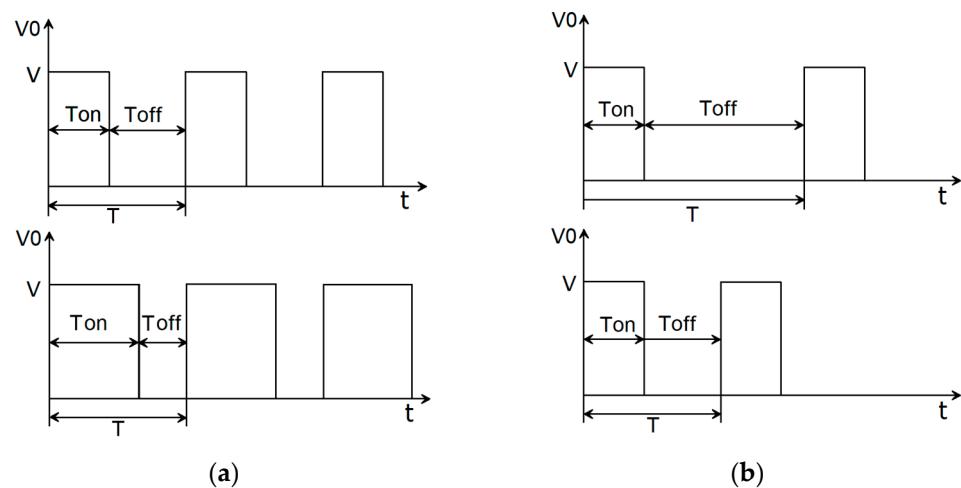
Figure 2. Pulse sequences at (**a**) PWM control and (**b**) VF control.

Examination of the DC–DC converter is conducted for operation state, where the current flow is continuous. This is the most common case in the practical implementations, where the circuit is used to deliver power from the source to the load and vice versa. Then, there are two main intervals of operation. The equivalent circuits are provided in Figure 3a,b.

(**a**)   (**b**)
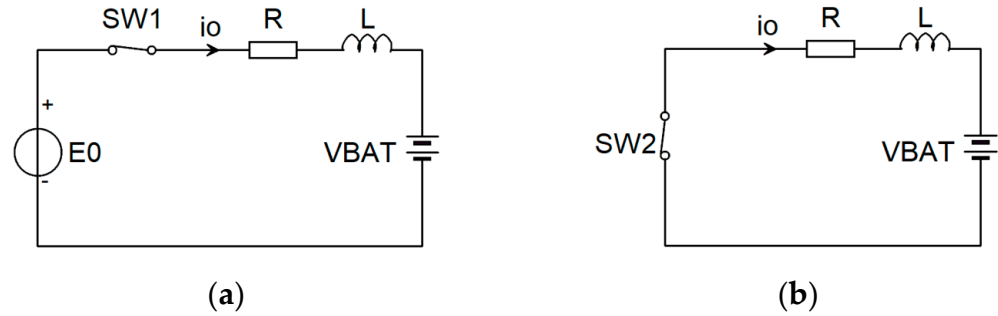
Figure 3. Equivalent circuit states at (**a**) period ON and (**b**) period OFF.

The following expressions are provided for two operation intervals of the DC chopper—Figure 3a, when modulating switch is ON ($0 \leq t \leq t_{on}$), and Figure 3b, when modulating switch is OFF. The expressions of load current i_0 and ripple voltage v_0 are provided below

$$E_0 = i_0 \cdot R + L\frac{d.i_0}{dt} + V_{BAT}. \tag{1}$$

Taking Laplace transform,

$$\frac{E_0}{S} = R \cdot I_0(S) + L\left[S \cdot I_0(S) - i_0\left(0^-\right)\right] + \frac{V_{BAT}}{S} \tag{2}$$

At $t = 0$, initial current $i_0(0^-) = I_{min}$

$$I_0(S) = \frac{E_0 - V_{BAT}}{LS\left(S + \frac{R}{L}\right)} + \frac{I_{min}}{S + \frac{R}{L}}. \tag{3}$$

Taking inverse Laplace transform,

$$i_0(t) = \frac{E_0 - V_{BAT}}{R}\left[1 - e^{-\left(\frac{R}{L}\right) \cdot t}\right] + I_{min}e^{-\left(\frac{R}{L}\right) \cdot t}. \tag{4}$$

The above expression is valid from ($0 \leq t \leq t_{on}$) during the period when modulating switch is ON. At the instant the switch is turned OFF, the load current is $i_0(t_{on}) = I_{max}$. When modulation switch is OFF ($0 \leq t \leq t_{off}$), we have the following expressions

$$0 = R \cdot i_0 + L\frac{di_0}{dt} + V_{BAT}. \tag{5}$$

Taking Laplace transform,

$$0 = R \cdot I_0(S) + L\left[S \cdot I_0(S) - i_0\left(0^-\right)\right] + \frac{V_{BAT}}{S}. \tag{6}$$

Redefining time origin we have at $t = 0$, the initial current $i_0(0^-) = I_{max}$

$$I_0(S) = \frac{I_{max}}{S + \frac{R}{L}} - \frac{V_{BAT}}{LS\left(S + \frac{R}{L}\right)}. \tag{7}$$

Taking inverse Laplace transform,

$$i_0(t) = I_{max}e^{-(\frac{R}{L})\cdot t} - \frac{V_{BAT}}{R}\left[1 - e^{-(\frac{R}{L})\cdot t}\right]. \tag{8}$$

The above expression is valid when ($0 \leq t \leq t_{off}$) during the period when modulating switch is OFF. At the instant the switch is turned OFF, load current is $i_0(0^-) = I_{min}$.

To find the values of I_{max} and I_{min}, we complete the following substitutions. From (4) at $t = t_{on} = dT$ and $i_0(t) = I_{max}$, we obtain

$$I_{max} = \frac{E_0}{R}\left[\frac{1 - e^{-\frac{dRT}{L}}}{1 - e^{-\frac{RT}{L}}}\right] - \frac{V_{BAT}}{R}. \tag{9}$$

From (8) at $t = t_{off} = (1 - d)T$ and $i_0(t) = I_{min}$, we obtain

$$I_{min} = \frac{E_0}{R}\left[\frac{e^{-\frac{dRT}{L}} - 1}{e^{-\frac{RT}{L}} - 1}\right] - \frac{V_{BAT}}{R}. \tag{10}$$

When we examine the circuit behavior in order to obtain the best possible component configuration and output filter design, we should consider the tolerance of the output variations and load variations. Just because the battery pack behavior of load is non-linear (battery parameters are dependent on current charge, temperature, ripple voltage, etc.), we consider output ripple values.

Ripple current $K_{p(i)}$ and voltage $K_{p(u)}$ could be determined by (11) and (12), while the effective output gain of the circuit β is provided in (13):

$$K_{p(i)} = \left(I_{max} - I_{min}\right)/2; \tag{11}$$

$$K_{p(u)} = \frac{E_0 \cdot d \cdot T}{R \cdot C_{BAT}} = \frac{E_0 \cdot d}{R \cdot C_{BAT} \cdot fsw}; \tag{12}$$

$$\beta = \frac{2L}{f_{sw} \cdot Z_{LOAD}} \tag{13}$$

where R is the overall circuit resistance, L is the inductor output filter value, C_{BAT} is the battery capacity, d is the duty factor, T is period of operation for fixed frequency and PWM control, while f_{sw} is the switching frequency, which is variable regarding VF control. Impedance of the load Z_{LOAD} is also unknown and changes during the operation. As a conclusion, in both cases of control approaches, we need proper output LC filter design in order to reduce the ripple and improve the circuit's overall efficiency.

3. Examination and Results

Authors used a mathematical approach for the LC output filter calculation with an excel model, which has been modified to determine the frequency response and loop gain reaction at variable loads. This is necessary because, in practical implementations, there is a solid relation between the load variations and circuit output stability. In order to determine the area of maximum efficiency over the different cases, several examinations have been processed. The exchange of the load impedance has been used in the tested application. In practice, the cell number and state of charge are also variable; therefore, the extract data for the examinations at different loads are provided. Some results are shown for the load factor deviation between 0.5 and 1. The extracted plots are presented for the single-ended LC filter configuration, which is typical for the DC chopper shown in Figure 1, consisting of an inductor L and capacitor C with the first pole of the configuration. The load capacity performance degrades for frequencies of current above the rated level. At higher frequencies, the capacitance behavior at higher frequencies is mostly resistive. It produces more power losses, thus reduce the life span of the capacitor. Therefore, it is producing

only power losses and reducing the capacitor's operation life span. Circuit output response is provided below as gain at rated frequency. The results are presented in Figure 4a–d. Figure 4a shows the output gain response at a load factor = 0.5. Figure 4b shows the output gain response at a load factor = 0.75. Figure 4c,d shows the output gain response at load factors equal to 0.9 and 1, respectively.

(**a**)

(**b**)

(**c**)

(**d**)
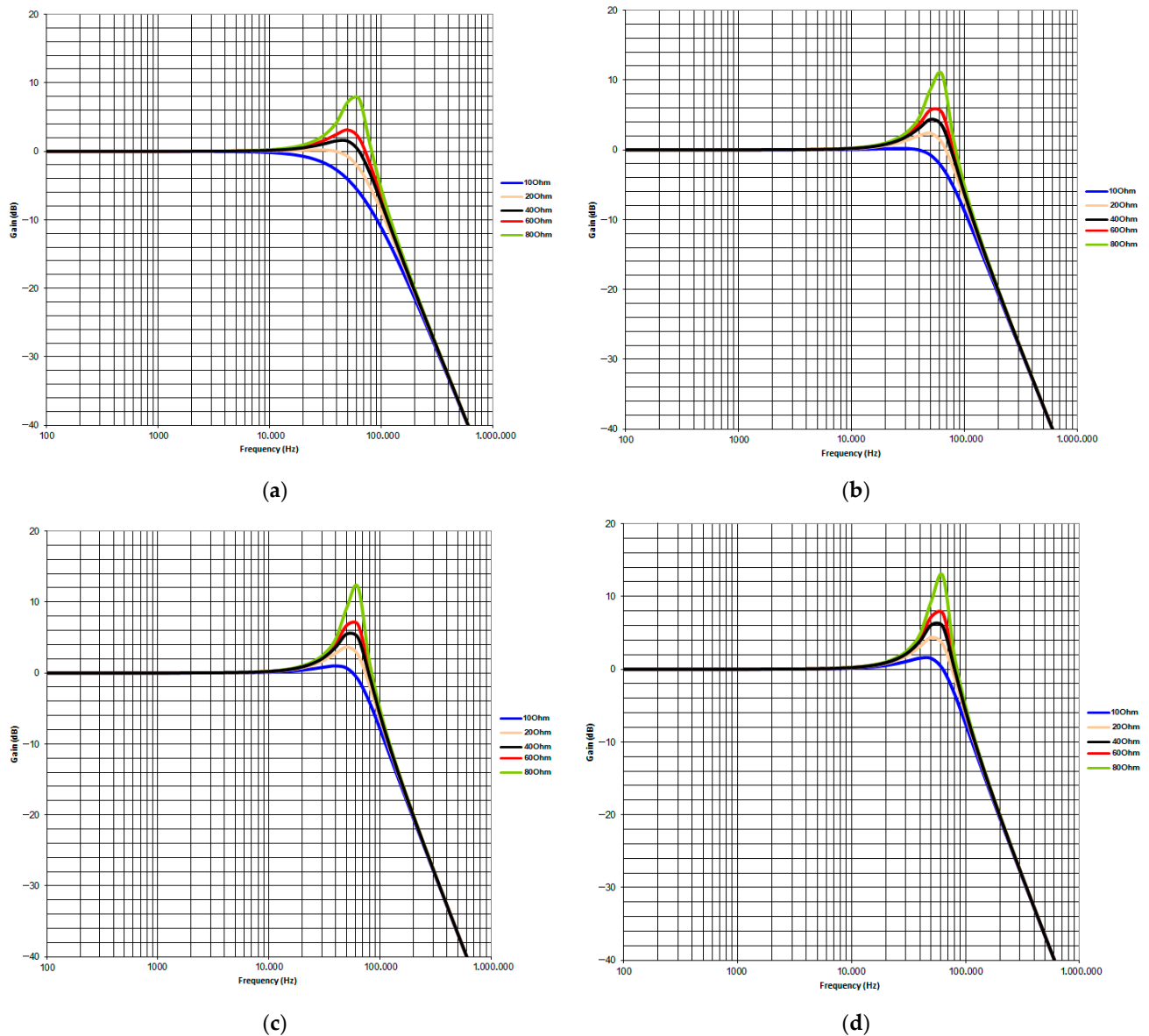
Figure 4. Circuit output gain at rated frequency and load factor variation: (**a**) at load factor 0.5, (**b**) at load factor 0.75, (**c**) at load factor 0.9 and (**d**) at load factor 1.

4. Conclusions

The examination results show that the DC–DC converter circuit behavior is relative and depends not only on the load exchange but also on the configuration of the output LC filter and its characteristics. The presented diagrams determine the state of operation, where the output values are controlled and steady. The flattened output response in the area between 10 KHz and 70 KHz shown in Figure 4a,b is crucial for most of the switching power applications. In this case, exchanging the working frequency above the rated level at the VF control could have a negative influence on the device stability. Considering this study, some more advanced control techniques, together with a closed-loop solution, can facilitate obtaining better results.

Furthermore, the simulations of the load variation show that the load factor could also have a significant impact on the circuit gain level at higher frequencies, where the capacity decreases and produces more active power losses and current ripple.

Through fixed working frequency PWM control, the provided calculations are mostly valid for the continuous mode of operation as a way to determine the ripple reduction and effectivity improvement. The presented approach of the investigation with a modified excel application could be used in some practical implementations where the load variations are unpredictable, and the calculations could have multiple changes to match the final revision.

The examination results show that the LC output filter design is important for current ripple reduction and improves the overall circuit effectivity. Some directions of future studies are related to the examination of different filter configurations with different circuit topologies and may include various practical implementations, either with passive or active filter topologies.

References

1. Massot-Campos, M.; Montesinos-Miracle, D.; Galceran-Arellano, S.; Rufer, A. Multilevel two quadrant DC/DC converter for regenerative braking in mobile applications. In Proceedings of the 2011 14th European Conference on Power Electronics and Applications, Bihrmingam, UK, 30 August–1 September 2011.
2. Zhao, B.; Yu, Q.; Sun, W. Extended Phase-shift Control of Isolated Bidirectional DC–DC Converter for Power Distribution in Microgrid. *IEEE Trans. Power Electron.* **2011**, *27*, 4667–4680. [CrossRef]
3. Kayaalp, R.İ.; Demirdelen, T.; Tümay, M. A novel fuzzy logic control for bidirectional DC-DC converter and comparison with dual phase-shift control method in medium voltage applications. In Proceedings of the IEEE International Conference on Computational Intelligence and Virtual Environments for Measurement Systems and Applications (CIVEMSA), Budapest, Hungary, 27–28 June 2016.
4. Altowati, A.; Zenger, K.; Suntio, T. Improved DC-DC Switching Power Converter Design Trough Modelling and Simulation. In Proceedings of the 47th Conference on Simulation and Modelling—SIMS 2006, Helsinki, Finland, 27–29 September 2006; pp. 74–76.
5. Indrasari, W.; Prasetya, F.A.I.; Setiadi, R.N. DC-DC Buck Converter Circuit Simulation on Solar Panel Electricity Storage System. *J. Phys. Conf. Ser.* **2021**, *2019*, 012091. [CrossRef]
6. Hou, N.; Li, Y.W. Overview and Comparison of Modulation and Control Strategies for Non resonant Single-phase Dual-active-bridge DC-DC converter. *IEEE Trans. Power Electron.* **2019**, *35*, 3148–3172. [CrossRef]
7. Husnain Ashfaq, M.; Al Selvaraj, J.; Abd Rahim, N. Control Strategies for Bidirectional DC-DC Converters: An Overview. *IOP Conf. Ser. Mater. Sci. Eng.* **2021**, *1127*, 012031. [CrossRef]
8. Nandankar, P.V.; Bedekar, P.P.; Kumar, P.; Dhawas, V. Variable switching frequency control for efficient DC-DC converter. *Mater. Today Proc.* **2022**, *51*, 515–521. [CrossRef]
9. Sobol, A.N.; Bogdan, A.V.; Uskov, A.E.; Denisenko, E.A. Methodology for simplified calculation of filter parameters of static power converters. *IOP Conf. Ser. Earth Environ. Sci. (TISA)* **2019**, *488*, 012040. [CrossRef]
10. Quek, Y.B. Class-D LC Filter Design. ti.com. Available online: https://www.ti.com/lit/pdf/slaa701 (accessed on 23 May 2024).